


## PAPER

[View Article Online](#)  
[View Journal](#) | [View Issue](#)Cite this: *Dalton Trans.*, 2023, **52**, 6536Carbon dioxide sequestration by mineral carbonation *via* iron complexation using bipyridine chelating ligands†Javier F. Reynes,<sup>a</sup> \*<sup>a</sup> Guy Mercier,<sup>b</sup> Jean-François Blais<sup>b</sup> and Louis-César Pasquier<sup>b</sup>

An innovative mineral carbonation method was developed to synthesize iron(II) carbonate ( $\text{FeCO}_3$ ) by cation complexation using 2,2'-bipyridine as ligand. First, complexes of iron(II) and different ligands were theoretically analyzed and discounted in terms of their temperature and pH-dependent stabilities, iron-ligand interactions, possible by-products and difficulty of analysis, choosing 2,2'-bipyridine as the most suitable ligand. Then, the Job plot was used to verify the complex formula. The stability of  $[\text{Fe}(\text{bipy})_3]^{2+}$  at pH 1–12 was further monitored for 7 days using UV-Vis and IR spectroscopy. Good stability was observed between pH 3 and 8, decreasing within pH 9–12 where the carbonation reaction occurs. Finally, the reaction between  $\text{Na}_2\text{CO}_3$  and  $[\text{Fe}(\text{bipy})_3]^{2+}$  was performed at 21, 60, and 80 °C and pH 9–12. The total inorganic carbon measured after 2 h shows that the best carbonate conversion (50%) occurred at 80 °C and pH 11, being the most suitable conditions for carbon sequestration. SEM-EDS and XRD were used to examine the effect of synthesis parameters on the morphology and composition of  $\text{FeCO}_3$ . The  $\text{FeCO}_3$  particle size increased from 10  $\mu\text{m}$  at 21 °C to 26 and 170  $\mu\text{m}$  at 60 and 80 °C respectively with no pH dependence. In addition, EDS analysis supported the carbonate identity, whose amorphous nature was confirmed by XRD. These results would help prevent the iron hydroxide precipitation problem during mineral carbonation using iron-rich silicates. These results are promising for its application as a carbon sequestration method with a  $\text{CO}_2$  uptake of around 50% obtaining Fe-rich carbonate.

Received 22nd February 2023,

Accepted 24th April 2023

DOI: 10.1039/d3dt00563a

[rsc.li/dalton](http://rsc.li/dalton)

## 1. Introduction

According to the latest reports by the Intergovernmental Panel on Climate Change (IPCC), the global greenhouse gas (GHG) emission has increased exponentially since the industrial revolution and by 70% from 1970 to 2004.<sup>1,2</sup> As a result, the average temperature increased by about 0.85 °C from 1880 to 2012. If this trend continues, the global average temperature will increase by 1–5 °C by 2100.<sup>3</sup>  $\text{CO}_2$  is the most abundant GHG showing the fastest growth rate, mainly due to the industrial combustion of fossil fuels and deforestation. For instance, the most recent values for global atmospheric  $\text{CO}_2$  levels provided by the National Oceanic and Atmospheric Administration (NOAA) *via* their global monitoring laboratory sets them in 419.31 ppm in January 2023, 82.75 ppm higher

than values from 1979 taken in the same month.<sup>4</sup> In order to achieve the IPCC targets, both industrialized and developing countries need to find ways to store  $\text{CO}_2$  that are affordable and easy to implement.

Iron carbonates, occurring naturally as the mineral siderite ( $\text{FeCO}_3$ ), have been studied recently as their potential to sequester  $\text{CO}_2$ .<sup>5</sup> Many routes have been proposed for synthesizing  $\text{FeCO}_3$ .<sup>6,7</sup> However, the most accepted method to prepare highly crystalline  $\text{FeCO}_3$  is the hydrothermal decomposition of  $\text{Fe(III)-EDTA}$  complex, starting from ferric ammonium sulfate and  $\text{Na}_4\text{EDTA}$  in the presence of urea.<sup>8–10</sup> Nevertheless, all these synthetic routes are too energy- or time-consuming for use in industrial  $\text{CO}_2$  capture.

A new chemical process, called mineral carbonation (MC), is based on the natural reaction between a divalent metal cation (mainly  $\text{Mg}^{2+}$ ,  $\text{Ca}^{2+}$ , and  $\text{Fe}^{2+}$ ) obtained mainly from silicates and dissolved  $\text{CO}_2$  to form stable carbonates.<sup>11–14</sup>

$\text{Fe(II)}$ -rich silicates, such as fayalite, have barely been studied, and investigations have been limited to the study of the aqueous mineral carbonation reaction under anoxic or supercritical  $\text{CO}_2$  conditions (185 °C and 150 bar) or high temperature and pressure conditions.<sup>15–17</sup> The main problem for iron carbonate precipitation is how to stabilize iron(II) cations in an aqueous solution at alkaline conditions. In the

<sup>a</sup>Departamento de Química Orgánica e Inorgánica, Facultad de Química, Universidad de Oviedo, Av. Julián Clavería, 8, 33006 Oviedo, Asturias, Spain.

E-mail: fernandezreyjavier@uniovi.es

<sup>b</sup>Institut National de la Recherche Scientifique (Centre Eau, Terre et Environnement), Université du Québec, 490 rue de la Couronne, Québec G1K 9A9, Canada

†Electronic supplementary information (ESI) available: Buffer solution preparation for each pH, additional UV-Vis spectra of the  $[\text{Fe}(\text{bipy})_3]^{2+}$  complex to show its long-term stability. See DOI: <https://doi.org/10.1039/d3dt00563a>

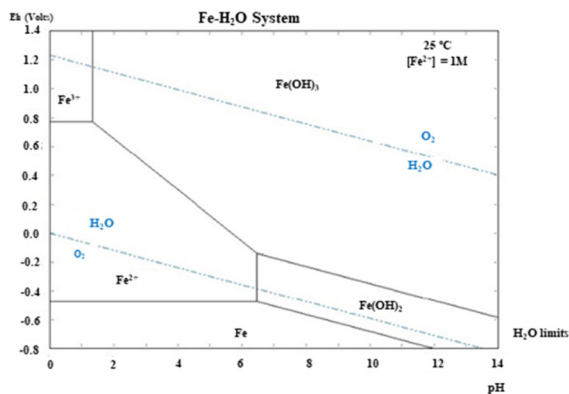


Fig. 1 Eh-pH diagram for the system of Fe–O–H at 25 °C and 1.00 bar total pressure, as calculated by HSC Chemistry 6.0.

Eh-pH diagram of iron species (Fig. 1), hydroxide precipitation starts at around pH 6, whereas that of  $\text{FeCO}_3$  occurs between pH 9 and pH 12.<sup>18</sup> It is then crucial to find an efficient way to maximize  $\text{FeCO}_3$  precipitation by stabilizing the iron(II) cation at high pH.

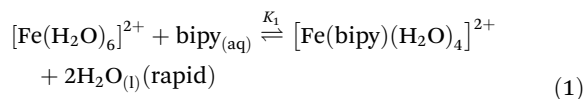
Ligand complexation is an obvious way to control the reactivity of metal ions.<sup>19,20</sup> Ligands have been used in many applications, such as bioinorganic chemistry,<sup>21</sup> medical chemistry,<sup>22</sup> homogeneous catalysis,<sup>23</sup> and metal removal from wastewater.<sup>24</sup> However, there are no reports on using ligands for MC reactions, due to the difficulty in finding an iron(II) complex that is stable in a wide pH window to allow  $\text{FeCO}_3$  precipitation. For example, ferrocyanide ( $[\text{Fe}(\text{CN})_6]^{4-}$ ) decomposes at alkaline pH to release very toxic cyanide ions.<sup>25</sup> In  $[\text{Fe}(\text{phen})_3]^{2+}$  and  $\text{Fe}(\text{II})$ -EDTA, the iron(II) is easily oxidized to form iron(III), and there is a strong tendency to form iron hydroxide precipitates.<sup>26–29</sup>

2,2'-Bipyridine may be a good ligand for the synthesis of iron carbonate, since it can form a very stable 3 : 1 mononuclear complex  $[\text{Fe}(\text{bipy})_3]^{2+}$  with the iron(II) ion. In this complex, iron(II) has a coordination number of 6 and is bonded to both nitrogen atoms in all three 2,2'-bipyridine. This complex is highly stable at alkaline pH and in a wide temperature range, neither does it interfere in the carbonation reaction. It also has a red color due to metal-to-ligand charge transfer (MLCT),<sup>19,30–32</sup> and so its stability can be easily monitored by monitoring the optical absorption at 522 nm.<sup>27,33,34</sup>

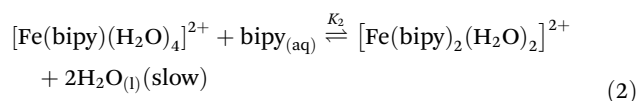
The stepwise formation of  $[\text{Fe}(\text{bipy})_3]^{2+}$  and the associated equilibrium constants are described in eqn (1)–(4).<sup>35</sup> Because iron(II) exists in the aqueous solution as a hydrated cation, the complexation by 2,2'-bipyridine is really a series of ligand exchange reaction to replace the coordinated water. Due to the effects of entropy, the first step of 2,2'-bipyridine's reaction with  $[\text{Fe}(\text{H}_2\text{O})_6]^{2+}$  is kinetically fast and also thermodynamically favorable, while the other two steps are much slower and less favorable. The overall formation constant (stability constant,  $\beta_3$ ) measures the tendency of the ligand and iron(II) to form  $[\text{Fe}(\text{bipy})_3]^{2+}$ , and it equals the product of the three individual stability constants  $K_1$ ,  $K_2$ , and  $K_3$  in eqn

(1)–(3). The value of  $\beta_3$  in eqn (4) suggests that  $[\text{Fe}(\text{bipy})_3]^{2+}$  is thermodynamically stable at standard conditions for temperature and pressure (STP).

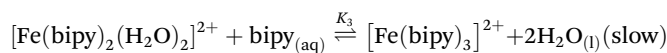
As we are not working on STP, these thermodynamic values can vary, so that the stability of the  $[\text{Fe}(\text{bipy})_3]^{2+}$  complex could be affected, crucial for the mineral carbonation reaction and the precipitation of the final iron carbonates. Fortunately, it has been demonstrated that the  $[\text{Fe}(\text{bipy})_3]^{2+}$  complex is very stable even when temperature is increased over 170 °C, with no appreciable changes in the stability constant  $\beta_3$ .<sup>36–38</sup> Nevertheless, in acidic conditions and higher temperatures, which is not the case in this study, the complex decomposed to give  $(\text{bipyH}_2)^{2+}$  and  $[\text{Fe}(\text{H}_2\text{O})_6]^{2+}$ , regenerating on cooling.<sup>36</sup>



$$K_1 = \frac{[\text{Fe}(\text{bipy})(\text{H}_2\text{O})_4]^{2+}}{[\text{Fe}(\text{H}_2\text{O})_6]^{2+} [\text{bipy}]}$$



$$K_2 = \frac{[\text{Fe}(\text{bipy})_2(\text{H}_2\text{O})_2]^{2+}}{[\text{Fe}(\text{bipy})(\text{H}_2\text{O})_4]^{2+} [\text{bipy}]}$$



$$K_3 = \frac{[\text{Fe}(\text{bipy})_3]^{2+}}{[\text{Fe}(\text{bipy})_2(\text{H}_2\text{O})_2]^{2+} [\text{bipy}]} \quad (3)$$

$$\beta_3 = K_1 \times K_2 \times K_3 = 24.3 \pm 0.9 \text{ L mol}^{-1} \text{ s}^{-1} \quad (4)$$

In this study,  $\text{FeCO}_3$  was newly synthesized *via* mineral carbonation by iron complexation with 2,2'-bipyridine. Experiments were carried out on the laboratory scale, using Mohr's salt ( $(\text{NH}_4)_2\text{Fe}(\text{SO}_4)_2 \cdot 6\text{H}_2\text{O}$ ) as the source of ferrous cation, 2,2'-bipyridine as ligand, and sodium carbonate ( $\text{Na}_2\text{CO}_3$ ) as carbonate source. The developed method has served to set a groundwork for its applications in developing efficient MC processes using Fayalite Fe-rich mining wastes and post-combustion  $\text{CO}_2$  in an aqueous medium at mild reaction conditions.<sup>39</sup>

## 2. Experimental section

### 2.1. Materials

The source chemicals were Mohr's salt ( $(\text{NH}_4)_2\text{Fe}(\text{SO}_4)_2 \cdot 6\text{H}_2\text{O}$ , 99%, ACS reagent), sodium carbonate ( $\text{Na}_2\text{CO}_3$ ,  $\geq 99.5\%$ , ACS reagent), and 2,2'-bipyridine ( $\geq 99\%$ , Sigma-Aldrich, ReagentPlus®).

### 2.2. Synthesis

Stock solutions of 2,2'-bipyridine and Mohr's salt (both 0.05 M) were separately prepared by dissolving 1.95 and 4.9 g of the



respective chemicals in 250 mL of deionized water. Around 10 mL of ethanol ( $\geq 99\%$ , Fisher Chemical) was added for the complete solubilization of 2,2'-bipyridine. A stock solution of  $[\text{Fe}(\text{bipy})_3]^{2+}$  (0.05 M) was synthesized by mixing together 62.5 and 187.5 mL of the Mohr's salt and 2,2'-bipyridine stock solutions, respectively. This  $[\text{Fe}(\text{bipy})_3]^{2+}$  solution was further diluted to 0.015 M with deionized water.

Different buffer solutions were prepared following the instructions given by ref. 40, and the details are listed in Table S1 of ESI† HCl and NaOH solutions (0.1 M each) were used to adjust the pH to the expected values.

A saturated solution of  $\text{Na}_2\text{CO}_3$  (2.89 M) was prepared by dissolving 76.75 g of  $\text{Na}_2\text{CO}_3$  in 250 mL of deionized water. After mixing 10 mL of this solution with  $[\text{Fe}(\text{bipy})_3]^{2+}$  (0.05 M, 25 mL), the precipitated iron carbonate was filtered and dried at 60 °C for 24 hours to obtain a red powder.

### 2.3. Characterization

To confirm the exact formula of the complex, the method of continuous variation (or Job plot) was employed. After mixing different molar fractions of Mohr's salt and 2,2'-bipyridine, a red complex solution was obtained, and the optical absorption of each one was measured at 522 nm (ref. 41) with 1 cm plastic cuvette using a UV-Vis spectrophotometer (Varian Cary 100 Bio UV-VIS, CA, USA).

The pH-dependent stability of the complexes was investigated using prepared buffer solutions (Table S1†) and UV-Vis spectroscopy measurements at 522 nm. The 0.05 M stock solution of  $[\text{Fe}(\text{bipy})_3]^{2+}$  was diluted to 0.015 M, in order to fit the UV-Vis absorbance range between 0–10 A. Tests were conducted over 7 days for each fixed pH between 1 and 12. The pH measurements (Accumet AR25 pH meter coupled with a Cole-Parmer pH platinum electrode, Fisher Scientific, NH, USA) were performed under constant stirring to ensure solution homogeneity. All analyses were carried out in triplicates. The pH-dependent stability was also studied by Fourier-transform infrared spectroscopy (FTIR; Cary 670 FTIR, CA, USA) by comparing with the standard infrared spectrum of  $[\text{Fe}(\text{bipy})_3]^{2+}$  at each pH.

Next,  $\text{FeCO}_3$  was precipitated by reacting the  $[\text{Fe}(\text{bipy})_3]^{2+}$  complex (0.05 M, 10 mL) with  $\text{Na}_2\text{CO}_3$  solution (2.89 M, 25 mL) at pH 9–12, an agitation speed of 250 rpm, and 25, 60, or 80 °C. Liquid samples were taken out at 0, 30, 60, and 120 minutes, and the total inorganic carbon (TIC) in them was analyzed (Shimadzu VCPH, Tokyo, Japan) to evaluate the reaction efficiency. After 2 hours of reaction, the sample solutions were filtered using a Büchner funnel and filter paper. The obtained iron carbonates were dried for 24 hours at 60 °C.

Scanning electron microscopy-energy dispersive spectroscopy (SEM-EDS; Zeiss EVO® 50 smart, Oberkochen, Germany) analyses were performed to study the samples' surface topology and elemental composition, thereby verifying the formation of iron carbonate.

X-Ray diffraction (XRD; Siemens D5000, MA, USA) was used to analyze the crystallinity and identify the mineral substance. The diffractometer was operated in the theta-theta configur-

ation using a copper radiation source. The obtained diffraction peaks were assigned by comparison with the JCPDS inorganic substances database.

## 3. Results and discussion

### 3.1. Characterization of the $[\text{Fe}(\text{bipy})_3]^{2+}$ complex

**3.1.1. Method of continuous variation or Job plot.** 2,2'-Bipyridine (0.5 M) and Mohr's salt (0.5 M) solutions were mixed in different mole fractions in order to study the stable stoichiometry of the complex. From the Job plot in Fig. 2 (mole fraction of Fe(II) vs. absorbance at 522 nm due to the red  $[\text{Fe}(\text{bipy})_3]^{2+}$ ), the highest absorbance (3.536) occurred when the molar fractions were  $X_{\text{Fe}^{2+}} = 0.25$  and  $X_{\text{bipy}} = 0.75$ . Therefore, the stable complex was confirmed to be  $[\text{Fe}(\text{bipy})_3]^{2+}$ , in agreement with the literature.<sup>41</sup>

**3.1.2. IR spectra.** Time-dependent IR spectra of 0.5 M  $[\text{Fe}(\text{bipy})_3]^{2+}$  complex solution were recorded within 3800–500  $\text{cm}^{-1}$  in the transmission mode at ambient temperature and the solution's natural pH (3.27). Fig. S1† shows the spectra as transmittance. When 2,2'-bipyridine is complexed to a metallic ion such as iron, its IR spectrum changes particularly in the regions 1650–1400  $\text{cm}^{-1}$  (C=N and C=C ring stretching vibrations) and 1050–850  $\text{cm}^{-1}$  (C–N out-of-plane deformations).<sup>42</sup> Those peaks were observed in the IR spectra here, supporting the formation of  $[\text{Fe}(\text{bipy})_3]^{2+}$  complex in the solution. Note that the broad peak near 3300  $\text{cm}^{-1}$  refers to C–H tensions of the complex.<sup>43</sup>

### 3.2. pH-Dependent stability of $[\text{Fe}(\text{bipy})_3]^{2+}$

The stability of  $[\text{Fe}(\text{bipy})_3]^{2+}$  complex over the pH range 1–12 was analyzed by measuring the absorbance at 200–700 nm, focusing on the characteristic peak of the complex at 522 nm in the visible region.<sup>41</sup> Two other absorbance peaks were also observed in the ultraviolet region between 200–350 nm. They come from the 2,2'-bipyridine ligand in solution regardless of complexation status, and therefore do not provide information about the complex's stability. Fig. 3 shows the UV-Vis spectra (400–700 nm) for 0.015 M  $[\text{Fe}(\text{bipy})_3]^{2+}$  complex in the pH range 1–12 measured on the day of mixing (day 1). The complex is not stable under strongly acidic conditions (pH 1, region III), although it is very stable within pH range 3–8

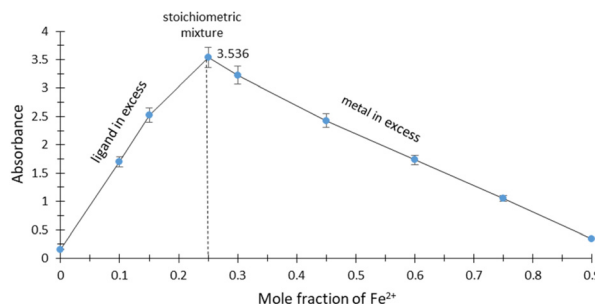


Fig. 2 Job's plot for the formation of  $[\text{Fe}(\text{bipy})_3]^{2+}$  complex.



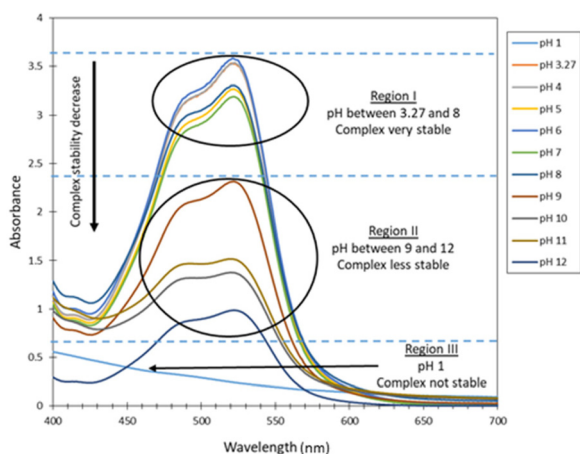


Fig. 3 UV-Vis spectra (400–700 nm) of  $[\text{Fe}(\text{bipy})_3]^{2+}$  complex solution (0.015 M) at pH 1–12 on day 1.

(region I). Note that a high stability between pH 5 and pH 8 is really important for retaining the complex in the solution during carbonation and avoiding iron hydroxide precipitation. Finally, in region II the stability decreases sharply from pH 9 to pH 12, where  $\text{FeCO}_3$  precipitation occurs. This weakening interaction between the ferrous cation and 2,2'-bipyridine facilitates reactions with the carbonate and bicarbonate ions in solution, leading to  $\text{FeCO}_3$  precipitation. The analysis was repeated during 7 days, but no further change in the complex stability was observed (Fig. S2†).

Based on the UV-Vis analysis performed and using the Beer's Law ( $A = \epsilon \cdot b \cdot c$ ), the concentrations of the  $[\text{Fe}(\text{bipy})_3]^{2+}$  at each pH were calculated in order to compare the differences in stability at each pH. The results are summarised in Table 1. Results highlight the low concentration of the complex at basic pH, which facilitates the reaction with the  $\text{CO}_3^{2-}$  ions and the final precipitation of  $\text{FeCO}_3$ .

The pH-dependent stability of the complex was also validated by monitoring the intensity of the characteristic IR peak at  $1045 \text{ cm}^{-1}$  (Fig. 4). As expected, the strongest peak can be

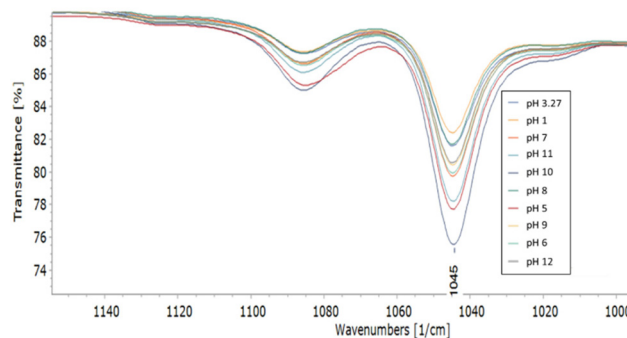


Fig. 4 IR spectra of  $[\text{Fe}(\text{bipy})_3]^{2+}$  solutions (0.5 M) at pH 1–12.

found at its natural pH (3.27), and the peak intensity (*i.e.*, complex stability) decreased at higher pH, except for pH 1.5 where the complex was the least stable. All these results are in concordance with the UV-Vis spectra, confirming the complex's stability in a wide range of pH over time.

### 3.3. $\text{FeCO}_3$ precipitation reaction

Having characterized the stability of  $[\text{Fe}(\text{bipy})_3]^{2+}$ , next we study the capacity of the carbonate ions to exchange with the 2,2'-bipyridine ligands for precipitating  $\text{FeCO}_3$ . Since only laboratory-scale experiments were conducted here, a pure chemical ( $\text{Na}_2\text{CO}_3$ ) was used as the carbonate source due to its high solubility in water even at high temperatures.<sup>44,45</sup>

The kinetic study was carried out in triplicate under different reaction conditions. For each condition,  $[\text{Fe}(\text{bipy})_3]^{2+}$  (0.5 M, 20 mL) was adjusted to the given pH (9, 10, 11, or 12), and stirred at 250 rpm while immersed in a water bath (25, 60, or 80 °C) under ambient pressure. After the desired temperature was reached, 10 mL of saturated 3.21 M  $\text{Na}_2\text{CO}_3$  solution was added. Then, samples were taken out after 0, 30, 60, and 120 minutes, and their TIC was measured to quantify the amount of  $\text{CO}_3^{2-}$  ions remaining in the solution. A larger reduction in  $\text{CO}_3^{2-}$  means a more efficient MC process. Note that, due to the very low solubility of  $\text{FeCO}_3$  in water ( $0.0067 \text{ g L}^{-1}$ ) with a  $K_{\text{sp}}$  of  $1.28 \times 10^{-11}$ ,<sup>46</sup> TIC measurement are very accurate to evaluate the effect of pH, temperature and time on the mineralization process because the  $\text{CO}_3^{2-}$  ions remaining in solution comes from the  $\text{Na}_2\text{CO}_3$  dissolved exclusively.

From the results in Table 2, a higher temperature enhances the reaction efficiency, as expected. Stronger thermal movement of the molecules would weaken the coordination interaction and accelerate carbonate formation.<sup>47</sup> Specifically, no significant change was found in the TIC at 25 °C even after 2 hours, meaning that hardly any iron carbonate was obtained. At 60 °C, the highest  $\text{FeCO}_3$  conversion was 25% at pH 10. Finally, when the temperature reached 80 °C, half of the carbonate ions precipitated as  $\text{FeCO}_3$  at pH 11 after 2 hours. The optimal pH can be explained by the complex's stability, which was very high at pH 9–10 and decreased at pH 11–12 (Fig. 3).

Table 1 Molar concentration of  $[\text{Fe}(\text{bipy})_3]^{2+}$  complex solution (0.015 M) at pH 1–12 on day 1

pH	Absorbance	Concentration (M)
1	Not stable	
3.27	3.50	0.0146
4	3.50	0.0146
5	3.20	0.0133
6	3.60	0.0150
7	3.10	0.0129
8	3.25	0.0136
9	2.30	0.0958
10	1.30	0.00541
11	1.50	0.00625
12	0.90	0.00375

Values were calculated based on Beer's Law ( $A = \epsilon \cdot b \cdot c$ ) with an optical path length ( $b$ ) of 1 cm and a molar absorption coefficient ( $\epsilon$ ) of  $240 \text{ M}^{-1} \text{ cm}^{-1}$  calculated based on the maximum absorbance.



**Table 2** Percentage of  $\text{CO}_3^{2-}$  ions remaining in the solution during carbonation

Temperature (°C)		21				60				80			
<i>t</i> (min)		0	30	60	120	0	30	60	120	0	30	60	120
pH	9	100	99.8	98.2	93.2	100	98.2	98.4	87.9	100	99.7	96.6	91.9
	10	100	91.6	90.9	88.1	100	99.3	86.6	75.9	100	97.6	97.4	85.6
	11	100	99.9	97.8	97.3	100	99.2	97.4	89.7	100	90.7	63.2	50.6
	12	100	97.7	97.7	95.2	100	97.8	88.1	85.2	100	93.3	77.3	63.0

TIC analysis (in %) were calculated by taking a 1 ml aliquot and dividing, based on the 3.21 M  $\text{Na}_2\text{CO}_3$  solution, the moles of  $\text{CO}_3^{2-}$  found by the initial ( $t = 0$ )  $\text{CO}_3^{2-}$  moles multiplying by 100.

### 3.4. $\text{FeCO}_3$ characterization

**3.4.1. SEM-EDS analysis.** After the 2 hours of reaction was finished, the solutions were cooled to ambient temperature if needed. The iron carbonates were obtained by filtration as a red solid due to trapped residual complex. A washing process was required to remove most of the  $[\text{Fe}(\text{bipy})_3]^{2+}$ , remaining the red color. After drying for 24 hours at 60 °C, the solid sample was divided into two portions: one for surface topography analysis by SEM, and the other for elemental analysis by EDS. These results are summarized in Fig. 6, where the EDS results (in wt%) were the average of 3 representative samples at each given temperature (21, 60, and 80 °C). In addition, EDS mapping results have been included in the ESI (Fig. S3†).

The sample morphology was explored using secondary electron (SE) imaging coupled to SEM, in order to provide important details about the particle surface, size and shape.

First of all, as the synthesis temperature rise, the particles size increased from 10  $\mu\text{m}$  at 21 °C to 26  $\mu\text{m}$  and 170  $\mu\text{m}$  at 60 °C and 80 °C respectively, where the grains were better defined. At ambient temperature, a magnification of 16 000–20 000 $\times$  was required to obtain a clear image. The corresponding magnification decreased to 7000–9000 $\times$  and 1500–5000 $\times$  at 60 and 80 °C, respectively. The more favorable reaction conditions (higher temperature and pH) destabilize the complex, help separate the iron from the ligand, and promote the iron's interaction with carbonate ions. On the other hand, the reaction pH does not significantly affect the particle size at a fixed temperature. The SEM images show the same morphology as that reported previously for iron carbonates.<sup>48</sup>

According to the EDS analysis (inset tables in Fig. 5 and Fig. S3†), the most abundant elements are iron (Fe), oxygen (O), and carbon (C) regardless of the reaction conditions, which are consistent with  $\text{FeCO}_3$ . However, the amount of C increased with the temperature from 3 to 8 wt%, which is expected to cause more efficient formation of  $\text{FeCO}_3$  by destabilizing the iron complex. Pure  $\text{FeCO}_3$  contains 10 wt% carbon, 42 wt% oxygen, and 48 wt% iron. The sample synthesized at 80 °C had a composition almost identical to the pure  $\text{FeCO}_3$  with 8, 39 and 44 wt% of C, O and Fe, respectively. These results agree with the TIC results (Table 2). Traces of sodium from  $\text{Na}_2\text{CO}_3$  also existed as an impurity. A purifi-

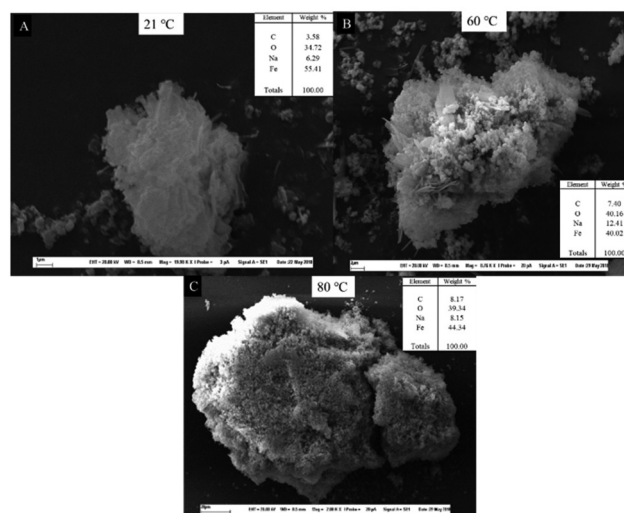


**Fig. 5** SEM images and EDS analysis (inset) of samples prepared at 21 °C (A) (19 980 $\times$ ), 60 °C (B) (8760 $\times$ ), and 80 °C (C) (2000 $\times$ ), using a polished section of the solid precipitate formed in the carbonation reaction.

cation step would be necessary to remove it from the solid product.

**3.4.2. XRD analysis.** Fig. 6 shows the XRD pattern of the product obtained under the optimum reaction conditions (pH

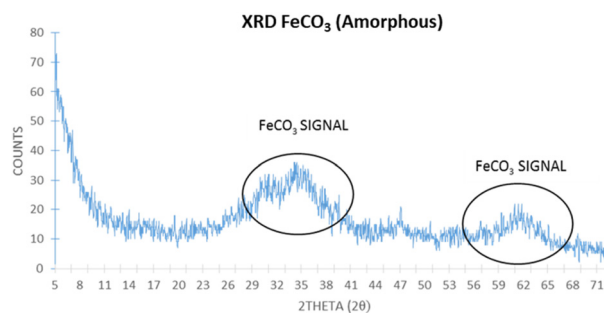


**Fig. 6** XRD pattern of  $\text{FeCO}_3$  precipitated during the carbonation reaction.



11 and 80 °C). Although the  $\text{FeCO}_3$  was not crystalline, there were nevertheless two peaks at around 32° and 60° that correspond to amorphous  $\text{FeCO}_3$ ,<sup>49</sup> reaffirming the results from TIC and SEM-EDS. Amorphous iron(II) carbonate (AFC) is a precursor of siderite (crystalline  $\text{FeCO}_3$ ). In the iron carbonate system, the speciation of Fe(II) ion has been shown to play a significant role in nucleation and/or precipitation in both chemical and geochemical environments. Conversely, in a reducing atmosphere, the formation of Fe(II) carbonate complexes contributes significantly to the speciation of Fe(II) ions.<sup>50</sup> Other chemical synthesis studies of siderite have suggested the formation of metastable precursors that dissolve at high temperature and pressure to give the crystalline end-product.<sup>51,52</sup> concluded that amorphous  $\text{FeCO}_3$  precursor provides a low-energy pathway for the crystallization of siderite, with an enthalpy of crystallization  $\Delta H_{\text{crystallization}} = -37.8 \pm 9.8 \text{ kJ mol}^{-1}$ . In developing MC reaction for  $\text{CO}_2$  sequestration, one should certainly consider the reservoir conditions such as a high pH (10–12), high temperature (50–100 °C), and high pressure (100–400 bar). Nevertheless, this reaction has been confirmed to be developed using mild conditions with good purity and yields both in batch and in a recirculation mode.<sup>39,53</sup>

## 4. Conclusions

An efficient  $\text{FeCO}_3$  precipitation procedure by iron complexation was developed. A red stable  $[\text{Fe}(\text{bipy})_3]^{2+}$  complex was prepared by simply mixing Mohr's salt and 2,2'-bipyridine in a molar ratio of 1 : 3. The stability of the  $[\text{Fe}(\text{bipy})_3]^{2+}$  complex between pH 1 and pH 12 was monitored for 7 days. The complex shows high stability at pH 3–8 and decreasing stability from pH 9–12, which is optimal for the carbonation reaction. Finally,  $\text{FeCO}_3$  was precipitated by mixing  $[\text{Fe}(\text{bipy})_3]^{2+}$  and a saturated  $\text{Na}_2\text{CO}_3$  solution. The precipitation efficiency over 2 hours of reaction time was studied at different pH (9–12) and temperatures (21, 60, and 80 °C) obtaining a maximum carbonate precipitation efficiency of 50% at pH 11 and 80 °C. SEM-EDS results confirmed the  $\text{FeCO}_3$  formation showing that the obtained particles were larger and better defined at higher temperatures with no changes with pH. Finally, XRD analysis revealed that the sample was amorphous  $\text{FeCO}_3$ . These results provide crucial information for the development of mineral carbonation reactions by cation complexation of Fe-rich mining wastes.

## Author contributions

Conceptualization, Javier F. Reynes, Guy Mercier, Jean-François Blais and Louis-César Pasquier; methodology, Javier F. Reynes, Guy Mercier, Jean-François Blais and Louis-César Pasquier; validation, Javier F. Reynes, Guy Mercier, Jean-François Blais and Louis-César Pasquier; formal analysis, Javier F. Reynes; investigation, Javier F. Reynes, Guy Mercier, Jean-François Blais and Louis-César Pasquier; resources, Javier

F. Reynes, Guy Mercier, Jean-François Blais and Louis-César Pasquier; data curation, Javier F. Reynes, Guy Mercier, Jean-François Blais and Louis-César Pasquier; writing—original draft preparation, Javier F. Reynes; writing—review and editing, Guy Mercier, Jean-François Blais and Louis-César Pasquier; visualization, Javier F. Reynes, Guy Mercier, Jean-François Blais and Louis-César Pasquier; supervision, Guy Mercier, Jean-François Blais and Louis-César Pasquier; project administration, Javier F. Reynes, Guy Mercier, Jean-François Blais and Louis-César Pasquier; funding acquisition, Guy Mercier, Jean-François Blais and Louis-César Pasquier. All authors have read and agreed to the published version of the manuscript.

## Conflicts of interest

The authors declare no conflict of interest. The funders had no role in the design of the study; in the collection, analyses, or interpretation of data; in the writing of the manuscript, or in the decision to publish the results.

## Acknowledgements

This research was funded by Fonds Québécois pour la Recherche et les Technologies (FQRNT), Programme de recherche en partenariat sur le développement durable du secteur minier, grant number 2017-MI-202241. I acknowledge all the support given for the production of this article including the administrative and technical support.

## References

- 1 C. De Klein, C. Pinares-Patino and G. Waghorn, *Environmental impacts of pasture-based farming*, ed. R. McDowell, 2008, pp. 1–33.
- 2 IPCC, *Climate Change 2007: Synthesis Report. Contribution of Working Groups I, II and III to the Fourth Assessment Report of the Intergovernmental Panel on Climate Change*, IPCC, Geneva, Switzerland, 2007.
- 3 IPCC, *Climate Change 2014: Synthesis Report. Contribution of Working Groups I, II and III to the Fifth Assessment Report of Intergovernmental Panel on Climate Change*, IPCC, Geneva, Switzerland, 2014.
- 4 NOAA, Global Monthly Mean  $\text{CO}_2$ , <https://gml.noaa.gov/ccgg/trends/global.html>, (accessed April, 11th, 2023).
- 5 M. Elsner, R. P. Schwarzenbach and S. B. Haderlein, *Environ. Sci. Technol.*, 2004, **38**, 799–807.
- 6 I. Llorens, M. Fattahi and B. Grambow, *MRS Online Proc. Libr. Arch.*, 2006, 985.
- 7 Y. Kim, Y. Lee and Y. Roh, *J. Nanosci. Nanotechnol.*, 2015, **15**, 5794–5797.
- 8 X. Feng, Q. Shen, Y. Shi and J. Zhang, *Ceram. Int.*, 2016, **42**, 14246–14251.
- 9 C. Zhang, W. Liu, D. Chen, J. Huang, X. Yu, X. Huang and Y. Fang, *Electrochim. Acta*, 2015, **182**, 559–564.



- 10 M. Chirita and A. Ieta, *Cryst. Growth Des.*, 2011, **12**, 883–886.
- 11 O. Rahmani, *J. CO<sub>2</sub> Util.*, 2018, **24**, 321–327.
- 12 K. S. Lackner, D. P. Butt and C. H. Wendt, *Energy Convers. Manage.*, 1997, **38**.
- 13 L.-C. Pasquier, G. Mercier, J.-F. Blais, E. Cecchi and S. Kentish, *Environ. Sci. Technol.*, 2014, **48**, 5163–5170.
- 14 O. Qafoku, L. Kovarik, R. K. Kukkadapu, E. S. Ilton, B. W. Arey, J. Tucek and A. R. Felmy, *Chem. Geol.*, 2012, **332–333**, 124–135.
- 15 C. Dimet, *Séquestration du CO<sub>2</sub> issu de l'industrie du fer par carbonatation minérale de résidus miniers et de roches mafiques : le cas de l'hématite et de la fayalite*, Université du Québec, Institut national de la recherche scientifique, 2016.
- 16 O. Qafoku, L. Kovarik, R. K. Kukkadapu, E. S. Ilton, B. W. Arey, J. Tucek and A. R. Felmy, *Chem. Geol.*, 2012, **332**, 124–135.
- 17 L. R. Penner, W. K. O'Connor, D. C. Dahlin, S. J. Gerdemann and G. E. Rush, *Mineral carbonation: energy costs of pretreatment options and insights gained from flow loop reaction studies*, Albany Research Center (ARC), Albany, OR (United States), 2004.
- 18 G. den Boef and A. P. Zuur, *Theoretische grondslagen van de analyse in waterige oplossingen*, Elsevier, 1980.
- 19 F. A. Cotton and G. Wilkinson, *Advanced inorganic chemistry*, Wiley, New York, 1988.
- 20 G. L. Miessler, P. J. Fischer and D. A. Tarr, *Inorganic Chemistry*, Published by Pearson, New Jersey, 2014, p. 682.
- 21 A. Ilin, B. Kerimzhanova and G. Yuldasheva, *J. Microb. Biochem. Technol.*, 2017, **9**, 293–300.
- 22 T. Storr, K. H. Thompson and C. Orvig, *Chem. Soc. Rev.*, 2006, **35**, 534–544.
- 23 B. Cornils, W. A. Herrmann, M. Beller and R. Paciello, *Applied Homogeneous Catalysis with Organometallic Compounds: A Comprehensive Handbook in Four Volumes*, John Wiley & Sons, 2017.
- 24 R. Abu-El-Halawa and S. A. Zabin, *J. Taibah Univ. Sci.*, 2017, **11**, 57–65.
- 25 E. Gail, S. Gos, R. Kulzer, J. Lorösch, A. Rubo, M. Sauer, R. Kellens, J. Reddy, N. Steier and W. Hasenpusch, *Journal*, 2012, **10**, 673–710.
- 26 D. Lazić, B. Škundrić, J. Penavin-Škundrić, S. Sladojević, L. Vasiljević, D. Blagojević and Z. Obrenović, *Chem. Ind. Chem. Eng. Q.*, 2010, **16**, 193–198.
- 27 P. Gülich, in *Metal Complexes*, Springer, 1981, pp. 83–195.
- 28 N. Sutin and B. Gordon, *J. Am. Chem. Soc.*, 1961, **83**, 70–73.
- 29 H. J. Wubs and A. A. Beenackers, *Ind. Eng. Chem. Res.*, 1993, **32**, 2580–2594.
- 30 D. M. Cabral, P. C. Howlett and D. R. MacFarlane, *Electrochim. Acta*, 2016, **220**, 347–353.
- 31 W. Gawelda, A. Cannizzo, V.-T. Pham, F. van Mourik, C. Bressler and M. Chergui, *J. Am. Chem. Soc.*, 2007, **129**, 8199–8206.
- 32 T. J. Meyer, *Pure Appl. Chem.*, 1986, **58**, 1193–1206.
- 33 M. A. Halcrow, *Crystals*, 2016, **6**, 58.
- 34 L. A. Paquette, D. Crich, P. Fuchs, G. Molander, A. R. Van Dyke and T. Jamison, *Encyclopedia of reagents for organic synthesis*, A. R. Van Dyke and T. F. Jamison, 2009.
- 35 A. M. Josceanu and P. Moore, *J. Chem. Soc., Dalton Trans.*, 1998, 369–374.
- 36 E. C. Constable and C. E. Housecroft, *Molecules*, 2019, **24**, 3951.
- 37 M. C. Carey, S. L. Adelman and J. K. McCusker, *Chem. Sci.*, 2019, **10**, 134–144.
- 38 S. Dhar and F. Basolo, *J. Inorg. Nucl. Chem.*, 1963, **25**, 37–44.
- 39 J. F. Reynes, G. Mercier, J.-F. Blais and L.-C. Pasquier, *Appl. Geochem.*, 2021, **131**, 105029.
- 40 R. A. Robinson and R. H. Stokes, *Electrolyte solutions*, Courier Corporation, 2002.
- 41 S. Xu, J. E. Smith and J. M. Weber, *Inorg. Chem.*, 2016, **55**, 11937–11943.
- 42 R. Khattak and I. I. Naqvi, *J. Res. Sci.*, 2007, **18**, 219–235.
- 43 B. D. Alexander, T. J. Dines and R. W. Longhurst, *Chem. Phys.*, 2008, **352**, 19–27.
- 44 M. Khan and S. Rogak, *J. Supercrit. Fluids*, 2004, **30**, 359–373.
- 45 E. Königsberger, L.-C. Königsberger and H. Gamsjäger, *Geochim. Cosmochim. Acta*, 1999, **63**, 3105–3119.
- 46 R. C. Wheast, *Handbook of chemistry and physics*, CRC press, 1983.
- 47 G. V. Gibbs, R. Downs, D. F. Cox, K. M. Rosso, N. L. Ross, A. Kirfel, T. Lippmann, W. Morgenroth and T. D. Crawford, *J. Phys. Chem. A*, 2008, **112**, 8811–8823.
- 48 A. Vuillemin, R. Wirth, H. Kemnitz, A. M. Schleicher, A. Friese, K. W. Bauer, R. Simister, S. Nomosatryo, L. Ordoñez and D. Ariztegui, *Geology*, 2019, **47**, 540–544.
- 49 S. Xuan, M. Chen, L. Hao, W. Jiang, X. Gong, Y. Hu and Z. Chen, *J. Magn. Magn. Mater.*, 2008, **320**, 164–170.
- 50 J. Bruno, W. Stumm, P. Wersin and F. Brandberg, *Geochim. Cosmochim. Acta*, 1992, **56**, 1139–1147.
- 51 W. W. Carothers, L. H. Adami and R. J. Rosenbauer, *Geochim. Cosmochim. Acta*, 1988, **52**, 2445–2450.
- 52 O. Sel, A. Radha, K. Dideriksen and A. Navrotsky, *Geochim. Cosmochim. Acta*, 2012, **87**, 61–68.
- 53 J. F. Reynes, G. Mercier, J.-F. Blais and L.-C. Pasquier, *Minerals*, 2021, **11**, 343.

